

Exploring the $\pi^+\pi^+$ Interaction in Lattice QCD

H.R. Fiebig^a, K. Rabitsch^b, H. Markum^b, A. Mithaly^c

^a Physics Department, FIU {University Park, Miami, Florida 33199, USA

^b Institut für Kernphysik, Technische Universität Wien, A-1040 Vienna, Austria

^c Department of Theoretical Physics, Lajos Kossuth University, H-4010 Debrecen, Hungary

(Revised 11-Nov-1999)

Abstract

An effective residual interaction for a meson-meson system is computed in lattice QCD. We describe the theoretical framework and present its application to the $I = 2$ channel S-wave interaction of the $\pi\pi$ system. Scattering phase shifts are also computed and compared to experimental results.

1 Introduction

For many decades boson exchange models have served as a theoretical basis for modeling the strong interaction [1]. This class of models has reached a high level of sophistication and has become a standard tool encompassing a large variety of strong interaction phenomena at low and intermediate energies [2]. On the other hand it has also become increasingly clear that quantum chromodynamics (QCD) provides the microscopic underpinnings for hadronic interaction.

The strong nuclear force operates in an energy range where the intrinsic hadronic ground states and a few excited states are important. At this low-to-intermediate energy scale the physics of QCD is only accessible through nonperturbative methods. While quark models have been used to capture part of the microscopic physics [3], there is no substitute for exploring hadronic interaction on a fundamental level. Currently the most appropriate way to do this is lattice field theory, supplemented by computational techniques.

As of today lattice QCD is well developed and explores many different topics ranging from quark confinement to hadron masses. Hadronic interactions, however, still have not moved into the mainstream of activity. Early work of Richards and collaborators [4, 5] addresses the role of quark exchange diagrams for meson-meson systems. Luscher's formula [6], which exploits finite-size effects, allows the extraction of scattering lengths from the lattice. It was applied to systems of pions and nucleons [7] within lattice QCD. Beyond static properties of two-hadron systems theoretical concepts become more involved. Luscher has devised a method [8] for relating the excitation spectrum of a two-body system in a finite box to scattering phase shifts. Elastic channel resonances are also within its scope [9]. Phase shifts become available for a discrete set of momenta. Discrete interpolation between those can be done through the use of different-sized lattices. Within an $O(4)$ symmetric ⁴ model extensive numerical tests [10] have shown that the method works well. However, unlike with the previous model, stringent numerical standards are much harder to meet for applications with QCD, where gauge fields and composite asymptotic states complicate the issue. In Luscher's method the 'master' equation that relates the two-body energy spectrum to scattering phases, unfortunately, has multiple solutions, the physical ones can be difficult to discern by solely numerical means.

In the nonrelativistic limit interactions can be described by potentials. Ongoing lattice work by Green and coworkers [11] focuses on geometric configurations of quarks in hadron-hadron systems and their interaction energies. A rather large body of work exists [11]–[16] with $SU(2)$ as the gauge group, including the heavy-light meson-meson system studied by Steward and Konik [17].

In $SU(3)$ a simple geometric model with static quarks tried by Rabitsch et al. [18] provides some exploratory insight into the gluon-generated part of the interaction

between two three-quark clusters. Extending this line of work, studies of heavy-light meson-meson systems were done [19] where the heavy quarks are treated as static and the light valence quarks are dynamic in the sense that their propagation is computed from the fermionic, staggered, lattice action. Although these studies are numerically difficult it appears that an attractive force between the partners is a common feature. However, in line with the exploratory flavor of these studies, the assignment of real-world quantum numbers to the hadronic systems was neglected.

Two-hadron systems with one infinitely heavy quark in each hadron have the advantage that their relative distance r is a theoretically well-defined notion. This opens the door to interactions of heavy-light systems. Still, realistic cases, involving B mesons for example, do require massive computing power. Most recently the UKQCD group has taken up simulations in this direction [20].

For light-light systems some work has been done in dimensions smaller than $d+1=4$ and gauge groups simpler than $SU(3)$. Probably the simplest nontrivial system in this class is a planar, $d=2$ lattice theory with a $U(1)$ gauge group. In finite volume, and with properly chosen coupling, β , the theory is confining. It can be used as a ‘toy’ system to develop techniques for studying hadronic interaction. This was done within the staggered fermion scheme for a meson-meson system [21]. In the nonrelativistic approximation a potential can be computed and used in a Schrodinger equation to calculate scattering phase shifts.

We will here follow essentially the ‘blueprint’ of [21] applying it to a $\{ \}$ system in the isospin $I=2$ channel. Using an $SU(3)$ gauge group in $d=3$ dimensions and a highly improved action we attempt a realistic calculation of the residual $\{ \}$ long-to-intermediate range interaction. Extrapolation to the chiral limit and a comparison of the corresponding scattering phase shifts to experimental results are performed.

Preliminary stages of this work have been reported before [22, 23]. A self-contained presentation of the formalism, in section 2, and a discussion and interpretation of the lattice results, in section 3, are the purpose of this paper.

2 Formalism

In the context of scattering within the framework of a quantum field theory the LSZ reduction formalism comes to mind. Putting the concept of ‘in’ and ‘out’ states, as $t \rightarrow \pm \infty$ in Minkowski time, to use in the Euclidean formulation proves, unfortunately, prone to theoretical difficulties. Maiani and Testa [24] studied a 3-point function $\langle h_{q_1}(t_1) q_2(t_2) J(0) \rangle$ involving a local source J and two fields interpolating a pseudoscalar particle. They showed that in the region $0 \leq t_2 \leq t_1$, of Euclidean times, the 3-point function depends only on the average (sum) of ‘in’ and ‘out’ matrix elements. Relative phases containing physical scattering information can thus not be extracted. This discouraging result, sometimes referred to as a no-go theorem, does not mean, how-

These operators describe two-meson systems with total momentum $\vec{P} = 0$ and relative momenta \vec{p} . They are designed to excite degrees of freedom of relative motion of the two composite mesons, in their respective intrinsic ground states. On a periodic lattice the momenta are

$$\vec{p} = \frac{2}{L}\vec{k} \quad \text{with} \quad \vec{k} \in \mathbb{R}^3 : \quad (3)$$

2.2 Correlation Matrices

Correlation matrices describe the propagation of the above fields in Euclidean time. Since we desire a comparison of the free (noninteracting) and the full (interacting) systems two types of correlation matrices are needed.

The time-correlation matrix for the one-meson system (2-point function) is

$$C_{\vec{p}\vec{q}}^{(2)}(\vec{t};\vec{t}_0) = \langle h_{\vec{p}}^y(\vec{t}) q_{\vec{q}}(\vec{t}_0) \rangle - \langle h_{\vec{p}}^y(\vec{t}) \rangle \langle q_{\vec{q}}(\vec{t}_0) \rangle; \quad (4)$$

with $\langle \cdot \rangle$ denoting the gauge-configuration average. In the usual way it is readily worked out by means of Wick's theorem

$$::: \overset{n}{\text{fsg}}(\vec{x}) \overset{n}{\text{fsg}}(\vec{y}) :::= ::: G^{\text{fsg}}(\vec{x};\vec{y}) :::; \quad (5)$$

where the pair n, n on the l.h.s. denotes the partners of a contraction. We assume the quark propagator G^{fsg} of the smeared fields to be flavor-independent

$$G_{fA, \vec{y}B}^{\text{fsg}}(\vec{x};\vec{y}) = \delta_{fA, B} G_{A, \vec{y}}^{\text{fsg}}(\vec{x};\vec{y}); \quad (6)$$

Since the smearing prescription used [26] does not mix flavor indices, (6) is a consequence of the corresponding relation of the unsmeared fields and thus holds independently of S , see Appendix A. We therefore will omit fsg from G to simplify notation. In (4) the separable term is zero, while there appear two contractions, $n = 1; 2$. Making use of translational invariance one obtains

$$C_{\vec{p}\vec{q}}^{(2)}(\vec{t};\vec{t}_0) = \delta_{\vec{p}\vec{q}} c_{\vec{p}}(\vec{t};\vec{t}_0) e^{i\vec{p} \cdot \vec{x}}; \quad (7)$$

with

$$c_{\vec{p}}(\vec{t};\vec{t}_0) = L^{-3} \sum_{\vec{x}} e^{i\vec{p} \cdot \vec{x}} \langle h_{A, \vec{y}}(\vec{x};\vec{x}_0\vec{t}_0) q_{\vec{y}}(\vec{x};\vec{x}_0\vec{t}_0) \rangle; \quad (8)$$

Sums over repeated indices are understood. The source point $\vec{x}_0 = (\vec{x}_0\vec{t}_0)$ is fixed and arbitrary. For later purposes we note that

$$c_{\vec{p}}(\vec{t};\vec{t}_0) = c_{\vec{p}}(\vec{t};\vec{t}_0); \quad (9)$$

The full meson-meson system propagates according to the 4-point function

$$C_{\vec{p}\vec{q}}^{(4)}(\vec{t};\vec{t}_0) = \langle h_{\vec{p}}^y(\vec{t}) q_{\vec{q}}(\vec{t}_0) \rangle - \langle h_{\vec{p}}^y(\vec{t}) \rangle \langle q_{\vec{q}}(\vec{t}_0) \rangle; \quad (10)$$

Working out the contractions here leads to a more complicated expression

$$\begin{aligned}
C_{pq}^{(4)}(t; t_0) = & L^{-12} \int_{x_1}^{x_2} \int_{y_1}^{y_2} e^{ip(x-x_1)+iq(y-y_1)} \\
& \times \int_{x_1}^{x_2} \int_{y_1}^{y_2} \left[G_{A_2 2; B_2 2}(x_2 t; y_2 t_0) G_{A_2 2; B_2 2}(x_2 t; y_2 t_0) \right. \\
& G_{A_1 1; B_1 1}(x_1 t; y_1 t_0) G_{A_1 1; B_1 1}(x_1 t; y_1 t_0) \\
& + G_{A_1 1; B_2 2}(x_1 t; y_2 t_0) G_{A_1 1; B_2 2}(x_1 t; y_2 t_0) \\
& G_{A_2 2; B_1 1}(x_2 t; y_1 t_0) G_{A_2 2; B_1 1}(x_2 t; y_1 t_0) \\
& G_{A_2 2; B_1 1}(x_2 t; y_1 t_0) G_{A_2 2; B_2 2}(x_2 t; y_2 t_0) \\
& G_{A_1 1; B_2 2}(x_1 t; y_2 t_0) G_{A_1 1; B_1 1}(x_1 t; y_1 t_0) \\
& G_{A_2 2; B_1 1}(x_2 t; y_1 t_0) G_{A_2 2; B_2 2}(x_2 t; y_2 t_0) \\
& \left. G_{A_1 1; B_2 2}(x_1 t; y_2 t_0) G_{A_1 1; B_1 1}(x_1 t; y_1 t_0) \right] : \quad (11)
\end{aligned}$$

Again, the separable term in (10) vanishes. Figure 1 shows the diagrammatic classi-

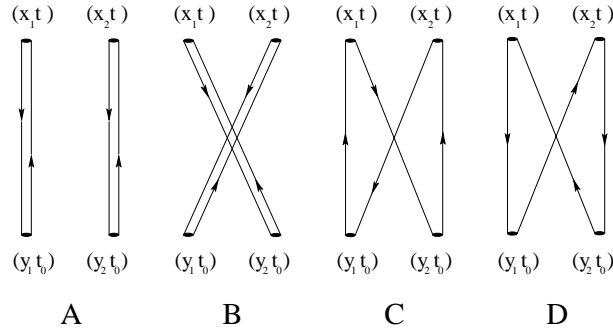


Figure 1: Diagrammatic classification of the full correlation matrix $C^{(4)}(t; t_0)$ according to (11)-(12).

cation of (11), leading to four terms

$$C^{(4)} = C^{(4A)} + C^{(4B)} + C^{(4C)} + C^{(4D)} : \quad (12)$$

It is useful to trace the pattern of contractions back to the 'meson content' of the correlators. Denoting the contractions as in (5) we write

$$C^{(4A)} = h \int_{+p}^{43} \int_{-p}^{21} \int_{+q}^{12} \int_{-q}^{34} i = h \int_{+p}^{43} \int_{+q}^{34} \int_{-p}^{21} \int_{-q}^{12} i \quad (13)$$

$$C^{(4B)} = h \int_{+p}^{21} \int_{-p}^{43} \int_{+q}^{12} \int_{-q}^{34} i = h \int_{-p}^{43} \int_{+q}^{34} \int_{+p}^{21} \int_{-q}^{12} i : \quad (14)$$

Each pair of equal numbers $n = 1 :: 4$ identifies contracted quark fields as they emerge from (1). Diagrams C and D exhibit valence quark exchange between the mesons

$$C^{(4C)} = h \sum_{+p} \gamma_{+p}^{23} \gamma_{-p}^{41} \gamma_{+q}^{12} \gamma_{-q}^{34} i \quad (15)$$

$$C^{(4D)} = h \sum_{+p} \gamma_{+p}^{41} \gamma_{-p}^{23} \gamma_{+q}^{12} \gamma_{-q}^{34} i; \quad (16)$$

and thus must be considered as sources of effective residual interaction.

We wish to extract from the full correlator $C^{(4)}$ a part which describes two composite 'lattice' mesons with their residual interaction switched off. This part is entirely contained in diagrams A and B, but gluonic correlations between the mesons are also present because the gauge configuration average $\langle \cdot \rangle$ is taken over the product of all four fields. Gluonic correlations contribute to the effective residual interaction. It is thus necessary to isolate the uncorrelated part contained in $C^{(4A)} + C^{(4B)}$.

2.3 Free Meson-Meson Correlator

Towards this end consider $C^{(4A)}$ in the form of (13). In the spirit of (5) we have

$$C^{(4A)} = \langle \sum_{+p} \gamma_{+p}^{43} \gamma_{-p}^{32} \gamma_{+q}^{21} \gamma_{-q}^{14} i \rangle; \quad (17)$$

where the $\langle \cdot \rangle$ indicates the Fourier sums, etc., which carry over from (1), see (11). The gauge configuration average in (17) may be analyzed in a systematic manner by means of cumulant expansion [27]. Taking advantage of $\langle \text{tr} G \rangle = 0$ we have

$$\langle \sum_{+p} \gamma_{+p}^{43} \gamma_{-p}^{32} \gamma_{+q}^{21} \gamma_{-q}^{14} i \rangle = \langle \sum_{+p} \gamma_{+p}^{43} \gamma_{-p}^{32} i \rangle \langle \sum_{+q} \gamma_{+q}^{21} \gamma_{-q}^{14} i \rangle + \langle \sum_{+p} \gamma_{+p}^{41} \gamma_{-p}^{23} i \rangle \langle \sum_{+q} \gamma_{+q}^{42} \gamma_{-q}^{31} i \rangle + \langle \sum_{+p} \gamma_{+p}^{43} \gamma_{-p}^{32} \gamma_{+q}^{21} \gamma_{-q}^{14} i \rangle; \quad (18)$$

The last term defines the cumulant. The first three terms on the right-hand side of (18) are illustrated in Fig. 2.

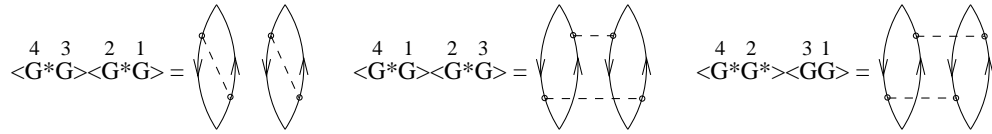


Figure 2: Illustration of the cumulant expansion of $C^{(4A)}$. The solid lines represent quark propagators, and the dashed lines gluonic correlations.

The dashed lines indicate that the quark propagators are correlated through gluons. Evidently only the first one of the three separable terms in (18) represents free, uncorrelated, mesons. All other terms are sources of effective residual interaction between

the mesons. We therefore define

$$\overline{C}^{(4A)} = h \begin{smallmatrix} 43 & 34 & 21 & 12 \\ + & p & + & q \end{smallmatrix} i h \begin{smallmatrix} 4 & 3 & 2 & 1 \\ p & q & p & q \end{smallmatrix} i : \quad (19)$$

A similar analysis of $C^{(4B)}$ leads to

$$\overline{C}^{(4B)} = h \begin{smallmatrix} 43 & 34 & 21 & 12 \\ + & p & + & q \end{smallmatrix} i h \begin{smallmatrix} 4 & 3 & 2 & 1 \\ p & q & p & q \end{smallmatrix} i : \quad (20)$$

The sum of those is the free meson-meson time correlation matrix

$$\overline{C}_{pq}^{(4)}(t; t_0) = \overline{C}_{pq}^{(4A)}(t; t_0) + \overline{C}_{pq}^{(4B)}(t; t_0); \quad (21)$$

which is an additive part of the full 4-point correlator

$$C^{(4)} = \overline{C}^{(4)} + C_I^{(4)}; \quad (22)$$

The remainder $C_I^{(4)}$, defined through (22), comprises all sources of the residual interaction, be it from gluonic correlations, or quark exchange (or quark-antiquark loops, if the simulation is unquenched).

The free correlator $\overline{C}^{(4)}$ describes two noninteracting identical lattice mesons. Their intrinsic structure is consistent with the dynamics determined by the lattice field model and its numerical implementation. Naturally, $\overline{C}^{(4)}$ may be expressed in terms of the 2-point correlator $C^{(2)}$. Using (4) and (19),(20) gives

$$\overline{C}_{pq}^{(4)} = C_{p\overline{q}}^{(2)} C_{p; q}^{(2)} + C_{p\overline{q}}^{(2)} C_{p; \overline{q}}^{(2)}; \quad (23)$$

Continuing with (7) and (9) this becomes

$$\overline{C}_{pq}^{(4)}(t; t_0) = (\delta_{p\overline{q}} + \delta_{p\overline{q}}) \mathcal{F}_p(t; t_0)^2; \quad (24)$$

It is interesting to note that the property

$$\overline{C}_{p\overline{q}}^{(4)} = \overline{C}_{p\overline{q}}^{(4)} = \overline{C}_{p; q}^{(4)} = \overline{C}_{p; \overline{q}}^{(4)}; \quad (25)$$

which is evident from (23), and also holds for $C^{(4)}$ through inspection of (11), reflects Bose symmetry with respect to the composite mesons. Permutation of the mesons, one with momentum $+p$ the other with momentum $-p$, results in the substitution $p \leftrightarrow -p$.

2.4 Residual Interaction

Eventually it would be desirable to extract scattering amplitudes, t-matrix elements, directly from a numerical simulation of lattice QCD. This would require a formulation of the LSZ prescription appropriate for the Euclidean lattice with the added complication that the asymptotic states are composites which themselves are determined by the

discretized quantum field theory and its specific numerical implementation. We are presently not aware of such a formulation.

For the time being we are content with defining an effective interaction from the computed lattice correlation matrices $C^{(4)}$ and $\overline{C}^{(4)}$ along the lines of Appendix B. We have in mind a description of the meson-meson system in terms of an effective Hamiltonian

$$H = H_0 + H_I; \quad (26)$$

where H_0 describes free propagation and H_I the residual interaction. We here adopt a definition of H_I suggested by an elementary Bose field theory subject to canonical quantization. In such a theory it is straightforward to calculate the perturbative expansion of $C^{(4)}$, as defined in (10) together with (2), but using elementary Bose fields instead. This is outlined in Appendix B. The zero-order term of the expansion corresponds to $\overline{C}^{(4)}$. Working up to second order we are lead to the following strategy:

Define an effective correlation matrix

$$C(t; t_0) = \overline{C}^{(4)}(t; t_0)^{1=2} C^{(4)}(t; t_0) \overline{C}^{(4)}(t; t_0)^{1=2} \quad (27)$$

$$= \overline{C}^{(4)}(t; t_0)^{1=2} C_I^{(4)}(t; t_0) \overline{C}^{(4)}(t; t_0)^{1=2} + \text{B bbl}; \quad (28)$$

where (22) was used for the alternative form.² Then in terms of C we define

$$H_I = \lim_{t \rightarrow 1} \frac{\partial \ln C(t; t_0)}{\partial t}; \quad (29)$$

To obtain H_I numerical diagonalization of the effective correlator matrix C is called for. The eigenvalues of C are expected to behave exponentially with t , thus rendering H_I a time-independent matrix.

In the numerical simulation it is desirable to utilize time slices with t as 'early' as possible in (29) since this gives smaller error bars. Towards this end the standard practice is to construct the interpolating fields from 'smeared' operators, see Appendix A. In this way the time correlation functions assume their asymptotic behaviour already at small t .

Another technique towards the same end was described in [28], and adopted in [10] for a lattice scattering problem. There, using the notation of [10] for the moment, the generalized eigenvalue problem $C(t)w = (t; t_0)C(t_0)w$ is considered. It leads to study the matrix $D(t; t_0) = C^{-\frac{1}{2}}(t_0)C(t)C^{-\frac{1}{2}}(t_0)$. This is an interesting parallel to the form of (27). It is stated in [10] that a reliable determination of the energy levels already for small values of t is achieved.

²Dividing out square roots of correlators $\overline{C}^{(4)}$ for composite free mesons bears some similarity to 'amputating' dressed external propagator lines.

2.5 Lattice Symmetry

From a numerical point of view computing C is greatly facilitated by utilizing symmetries of the lattice. The action used with our L^3 T lattice is invariant under the group $O(3;Z)$ of discrete transformations of the cubic sublattice. Using common notation [29] the irreducible representations are $\underline{0} = A_1; A_2; E^+; T_1; T_2$ with respective dimensionalities $N = 1; 1; 2; 3; 3$.

Given a fixed discrete lattice momentum \underline{p}^0 , see (3), the application of all group transformations $g \in O(3;Z)$ generates a set of momenta $\underline{p} = O_g \underline{p}^0$ which all have the same length $p = |\underline{p}^0|$. These transformations define a representation of $O(3;Z)$, say its basis vectors are $|\underline{p}\rangle$, which is in general reducible. Let

$$|\underline{p}\rangle = \sum_{\alpha} \sum_{\beta} j(\alpha; p) |\alpha\rangle \langle \beta; p| |\underline{p}\rangle; \quad (30)$$

with $j(\alpha; p) |\alpha\rangle$, $\alpha = 1 :: N$, being a set of basis vectors of the subspace that belongs to \underline{p} . Systematic construction of those basis vectors is straightforward [29]. For example, choosing an on-axis momentum $\underline{p}^0 = (p; 0; 0)$, and $\underline{0} = A_1^+$, one obtains

$$j(A_1^+; 0) |\alpha\rangle = j(0; 0; 0) |\alpha\rangle \quad \text{for } p = 0 \quad (31)$$

$$j(A_1^+; p) |\alpha\rangle = \frac{1}{6} \sum_{\beta} (j(\beta; p; 0) |\alpha\rangle + j(0; \beta; p) |\alpha\rangle + j(0; 0; \beta) |\alpha\rangle) \quad (32)$$

for $p > 0$:

It is also useful to know that representations \underline{l} of the continuum group $O(3)$ characterized by their angular momentum $\underline{l} = 0; 1 :: 4$ have decompositions

$$\begin{aligned} \underline{0} &= A_1^+ \\ \underline{1} &= T_1 \\ \underline{2} &= E^+ \quad T_2^+ \\ \underline{3} &= A_2 \quad T_1 \quad T_2 \\ \underline{4} &= A_1^+ \quad E^+ \quad T_1^+ \quad T_2^+; \end{aligned} \quad (33)$$

if $\underline{l} > 4$ the last four lines apply cyclically. The above follows from letting $O(3;Z)$ operate on harmonic polynomials $r^l Y_m(\underline{r})$ which form a basis for \underline{l} .

Since both the full and the free correlators $C^{(4)}$ and $\overline{C}^{(4)}$, respectively, commute with all group operations $g \in O(d;Z)$ there exist reduced matrices, say $C^{(4; \underline{l})}$ and $\overline{C}^{(4; \underline{l})}$, within each irreducible representation \underline{l} such that

$$\langle \alpha; p | \mathcal{J}^{(4)}(\underline{t}; \underline{t}_0) j(\underline{0}; \underline{q})^0 \rangle = \delta_{\alpha 0} C_{pq}^{(4; \underline{l})}(\underline{t}; \underline{t}_0) \quad (34)$$

and similarly for $\overline{C}^{(4; \underline{l})}$. It is obvious from (24) and (25) that the reduced matrix elements of the free correlator have the form

$$\overline{C}_{pq}^{(4; \underline{l})}(\underline{t}; \underline{t}_0) = \rho_{pq} c_p^{(\underline{l})}(\underline{t}; \underline{t}_0)^2; \quad (35)$$

The functions $c_p^{(4)}(t; t_0)$ are related to $c_p(t; t_0)$ by a p - and t -dependent factor. The above representation of $\bar{C}^{(4)}$ is of great advantage for numerical work because the inverse-square-root operation needed to compute the effective correlator (27) is now trivial. In the sector we simply have

$$C_{pq}^{(4)}(t; t_0) = \frac{C_{pq}^{(4)}(t; t_0)}{\phi^{(4)}(t; t_0) \bar{q}^{(4)}(t; t_0)} : \quad (36)$$

We envision numerical diagonalization, say

$$C_{pq}^{(4)}(t; t_0) = \sum_{n=1}^X v_n^{(4)}(p) \phi_n^{(4)}(t; t_0) v_n^{(4)}(q) : \quad (37)$$

For asymptotic times the eigenvectors $v_n^{(4)}$ are time independent [28], whereas the eigenvalues behave exponentially

$$\phi_n^{(4)}(t; t_0) = \bar{q}_n^{(4)} \exp(-w_n^{(4)}(t - t_0)) : \quad (38)$$

It is worth noting that diagonalization on each time slice, if numerically feasible, ensures that excited states decouple from the ground state, and each other, by virtue of orthogonal eigenvectors. Thus, at least for a large enough size of $C^{(4)}$, the $t \rightarrow 1$ behavior avoids the two-body relative ground state.

Extracting the effective residual interaction as defined in (29) now becomes a trivial matter. Provided that the $v_n^{(4)}$ are orthonormal we have

$$H_{I,pq}^{(4)} = \sum_{n=1}^X v_n^{(4)}(p) w_n^{(4)} v_n^{(4)}(q) : \quad (39)$$

These are the desired matrix elements of the effective residual interaction in the sector. In the basis $|p\rangle$ of lattice momenta we have

$$\langle p | H_{I,pq}^{(4)} | q \rangle = \sum_{n=1}^X \langle p | j(i; p) \rangle H_{I,pq}^{(4)} \langle (i; q) | q \rangle : \quad (40)$$

How many irreducible representations of the cubic lattice symmetry group actually are needed in the above series depends on the hadron-hadron system under consideration, the kinematical conditions, and on the partial waves that couple into the total spin J of the system. In this context the decompositions (33) become relevant.

In the numerical part of this work only the sector $= A_1^+$ is considered.

2.6 Nonrelativistic Potentials

From a kinematical point of view a $\{ \}$ system is ill suited for a description by non-relativistic potentials. Despite to-be-expected strong relativistic effects there are still

good reasons, however, to pursue this venue. First, we expect a potential to give insight into the nature of the residual interaction (attractive, repulsive, range, etc.). Second, a lattice simulation typically is performed in the realm of large pseudoscalar mass, certainly larger than the physical mass. In this region the potential picture still may have some validity. It is only through extrapolation that the relativistic region will be reached. Third, it seems that the shortage of lattice work in the area of hadron-hadron interaction, particularly for real-world systems, lends some justification to drastic approximations, at this stage.

The coordinate space matrix elements of the effective residual interaction are obtained from (40) by discrete lattice Fourier transformation. After redefining momentum variables we have

$$\langle \mathbf{x} | H_I | \mathbf{p} \rangle = L^{-3} \sum_{\mathbf{p}'} \sum_{\mathbf{q}} e^{i\mathbf{p}' \cdot (\mathbf{x} - \mathbf{s})} e^{i\mathbf{q} \cdot (\mathbf{x} + \mathbf{s})} \langle \mathbf{p}' - \mathbf{q} | H_I | \mathbf{p} + \mathbf{q} \rangle : \quad (41)$$

It is useful to write the matrix element of H_I as a sum of $\langle \mathbf{q} | H_I | \mathbf{p} + \mathbf{q} \rangle$ and a remainder. A reference system where the relative momenta before and after a scattering event are \mathbf{q} , respectively, is known as the Breit frame [30]. Then, the sum over \mathbf{p}' in (41) gives rise to $\delta_{\mathbf{x}, \mathbf{s}}$ and thus to a local operator $V(\mathbf{x})$ for the Breit-frame contributions, and a genuinely nonlocal operator $W(\mathbf{x}; \mathbf{s})$ for the remainder

$$\langle \mathbf{x} | H_I | \mathbf{p} \rangle = \delta_{\mathbf{x}, \mathbf{s}} V(\mathbf{x}) + W(\mathbf{x}; \mathbf{s}) : \quad (42)$$

Effectively, V and W comprise all microscopic dynamical effects, ultimately by way of the lattice action, that possibly contribute to the residual interaction between the composite mesons. Loosely speaking, these include potential as well as kinetic (hopping) effects. In a quantum field theory this distinction hardly makes sense, however, there exists an interesting parallel in the many-body theory of nuclear reactions. There, techniques known as resonating group method (RGM) and the essentially equivalent generator coordinate method (GCM) lead to effective interactions between composite nuclei which are built from both kinetic and potential energies of some microscopic Hamiltonian. The brief digression of Section 2.6.1 will illuminate the analogy.

Following common semantics we will refer to V and W as potentials. Their particular forms are

$$V(\mathbf{x}) = \sum_{\mathbf{q}} e^{i2\mathbf{q} \cdot \mathbf{x}} \langle \mathbf{q} | H_I | \mathbf{p} + \mathbf{q} \rangle \quad (43)$$

$$W(\mathbf{x}; \mathbf{s}) = L^{-3} \sum_{\mathbf{p}'} \sum_{\mathbf{q}} e^{i\mathbf{p}' \cdot (\mathbf{x} - \mathbf{s})} e^{i\mathbf{q} \cdot (\mathbf{x} + \mathbf{s})} (\langle \mathbf{p}' - \mathbf{q} | H_I | \mathbf{p} + \mathbf{q} \rangle - \langle \mathbf{q} | H_I | \mathbf{p} + \mathbf{q} \rangle) : \quad (44)$$

We will here limit ourselves to the relative S-wave local potential. Projecting (43) onto the partial wave $\ell = 0$,

$$V_0(x) = \frac{1}{4} \int_{-Z}^Z d\mathbf{x} V(\mathbf{x}) ; \quad (45)$$

implies a prescription for interpolation between the lattice sites. Whereas \mathbf{r} in (43) is assumed discrete it has been reinterpreted as a continuous variable for the purpose of integration in (45). The effect of the angular integration on (43) is that only diagonal A_1^+ sector reduced matrix elements of the expansion (40) survive. We have

$$V_0(\mathbf{r}) = \sum_q^X j_0(2qr) H_{I,qq}^{(A_1^+)}; \quad (46)$$

where $j_0(x) = \sin(x)/x$. Note that the sum in (46) runs over discrete lattice momenta.

2.6.1 Succinct RGM

We divert to specify the analogies mentioned above. The resonating group method (RGM), and its cousin the generator coordinate method (GCM), are specially applicable to a system of two composite nuclei. For the many-body wave function of two nuclei, say 1 and 2, the RGM ansatz is $\Psi = A(\phi_1(\mathbf{r}_1)\phi_2(\mathbf{r}_2)g(\mathbf{r}))$, where $\mathbf{r}_{1,2}$ are intrinsic coordinates and \mathbf{r} is the relative coordinate between the clusters. The operator A antisymmetrizes with respect to nucleon exchange. The microscopic Hamiltonian operator H , with $AH = HA$, can be written as $H = H_1 + H_2 + T_{12} + V_{12}$ where $H_{1,2}$ refer to the intrinsic degrees of freedom and T_{12}, V_{12} are the relative kinetic and potential energy operators. While $\phi_{1,2}$ are input, for example shell-model wave functions, the relative wave function $g(\mathbf{r})$ is subject to solution of the RGM equation $\langle \phi_1 \phi_2 | \mathbf{r} | (H - E) A | \phi_1 \phi_2 | g \rangle = 0$, all \mathbf{r} , where $\mathbf{r}(\mathbf{r}) = \delta^3(\mathbf{r} - \mathbf{r})$. In terms of the integral kernels $n(\mathbf{r}; \mathbf{r}^0) = \langle \phi_1 \phi_2 | \mathbf{r} | A | \phi_1 \phi_2 | \mathbf{r}^0 \rangle$ and $h(\mathbf{r}; \mathbf{r}^0) = \langle \phi_1 \phi_2 | \mathbf{r} | H A | \phi_1 \phi_2 | \mathbf{r}^0 \rangle$ the RGM equation reads $(h - E n)g = 0$. Assuming that the so-called overlap kernel n has no zero eigenvalues (redundant states) it can be cast into the form of a Schrodinger equation. Defining

$$h_{\text{RGM}} = n^{-1/2} h n^{-1/2}; \quad (47)$$

we have $(h_{\text{RGM}} - E)f = 0$ with $f = n^{1/2}g$. Here $h_{\text{RGM}} = h_0 + h_I$ is an effective Hamiltonian for the two-nucleus system. Its free part, h_0 , stems from splitting off terms with no rest antisymmetrization, direct terms, in this case the first terms in $A = 1 - (1 - A)$ and $HA = (H_1 + H_2 + T_{12}) + V_{12} + H(A - 1)$ in the definitions of $n(\mathbf{r}; \mathbf{r}^0)$ and $h(\mathbf{r}; \mathbf{r}^0)$, respectively, and also in $n^{-1/2} = 1 + (n^{-1/2} - 1)$. Direct terms lead to local operators on the wave function $f(\mathbf{r})$. In this way $(h_{\text{RGM}} - E)f = 0$ assumes the form

$$\frac{\hbar^2}{2m_{12}} \nabla^2 f(\mathbf{r}) + V_{\text{RGM}}(\mathbf{r}) f(\mathbf{r}) + \int d^3r^0 W_{\text{RGM}}(\mathbf{r}; \mathbf{r}^0) f(\mathbf{r}^0) = (E - E_1 - E_2) f(\mathbf{r}); \quad (48)$$

Here m_{12} is the reduced mass, the kinetic operator is identical with T_{12} , and $E_{1,2}$ are the internal cluster energies. Microscopic dynamics with kinetic and potential energies, contained in H , are cast into the effective potentials $V_{\text{RGM}}; W_{\text{RGM}}$.

Analogies with (26) and (42) suggest themselves. Since the spectrum of H_0 is akin to $2\sqrt{m^2 + p^2} = 2m + p^2/m + \dots$, similarities exist between $E_1 + E_2 - \frac{h^2}{2m_{12}} x$ and H_0 , and between $V_{\text{RGM}}; W_{\text{RGM}}$ and $V; W$ or H_I . Loosely speaking $2m$ plus the relative kinetic energy of our two-pion system drops out in the ratio of (27).

3 Computational Issues, Analysis and Results

The numerical implementation poses some extraordinary challenges. Compared to typical hadronic mass scales, energy shifts due to residual interaction can be quite small. On the other hand, the total energies of a two-hadron system at larger relative momenta tend to be big. Thus extracting energy shifts from ratios, see (36), of steeply dropping time correlation functions can push the numerical quality of the lattice simulation to its limits.

3.1 Lattice Implementation

The computation has been done on an $L^3 \times T = 9 \times 13$ lattice. We have used a tree-level $O(a^2)$ tadpole improved next-nearest-neighbor action, as discussed in [31, 32], in a quenched simulation. The number of gauge configurations was $N_{\text{U}} = 208$ separated by at least 1024 update steps. The hadron spectrum of this action has been studied in [33], and also in [34], on coarse lattices. Quite good agreement with the experimental masses was observed in both cases. In the conventions of [33] the gauge field coupling parameter was $\beta = 6.2$. This corresponds to a lattice constant of

$$a \approx 0.4 \text{ fm} \quad \text{or} \quad a^{-1} \approx 0.5 \text{ GeV} \quad (49)$$

as determined from the string tension³. This lattice is rather coarse, on the other hand a large lattice volume (here $L a \approx 3.6 \text{ fm}$) is required to accommodate two hadrons and to allow for sufficiently large separations at which their residual interaction becomes negligible.

The fermion part of the improved action [33] contains the Wilson hopping parameter κ . Quark propagators were obtained for the six values

$$\kappa^{-1} = 5.720; 5.804; 5.888; 5.972; 6.056; 6.140; \quad (50)$$

using a multiple mass algorithm [35]. The critical value for κ^{-1} is about 5.5. The correlator matrix (11) requires quark propagator matrix elements $G(x; y, t_0)$ between arbitrary lattice sites, except that the initial time slice is fixed. Computing all of those is not feasible. A random source technique very similar to the one described in [36]

³ Unless otherwise noted all lengths and energies are given in units of a and a^{-1} , respectively, throughout the text and the figures.

was employed, see Appendix A. The number of complex Gaussian random sources was $N_R = 8$ for each color-Dirac source point, thus we effectively have $8 \times 3 \times 4 = 96$ random sources per gauge configuration available to estimate G .

The fermion fields were subjected to Gaussian smearing'. We have used the smearing strength parameter $\alpha = 2$, in the notation of [26], and $S = 4$ iterations for smearing at the sink. This parameter set is similar to the one used in [33] with the same type action. In addition 'APE fuzzing' [37], which is the analogue of smearing for link variables, was done on each gauge configuration prior to smearing, also with $\alpha = 2$ and $S = 4$.

3.2 Correlator Analysis

The centerpiece of the numerical effort is the effective correlator matrix (36). We have computed $5 \times 5 A_1^+$ -sector matrices $C^{(4A_1^+)}(t; t_0)$ and $\bar{C}^{(4A_1^+)}(t; t_0)$ for on-axis momenta

$$q = \frac{2}{L}k \quad \text{with } k = 0; 1; 2; 3; 4: \quad (51)$$

The source time slice is at $t_0 = 3$. It turns out that the $C^{(4A_1^+)}(t; t_0)$ are dominated by their diagonal elements. The off-diagonal elements are small and have somewhat large statistical errors, mostly extending across zero. Hence it is reasonable to adopt the

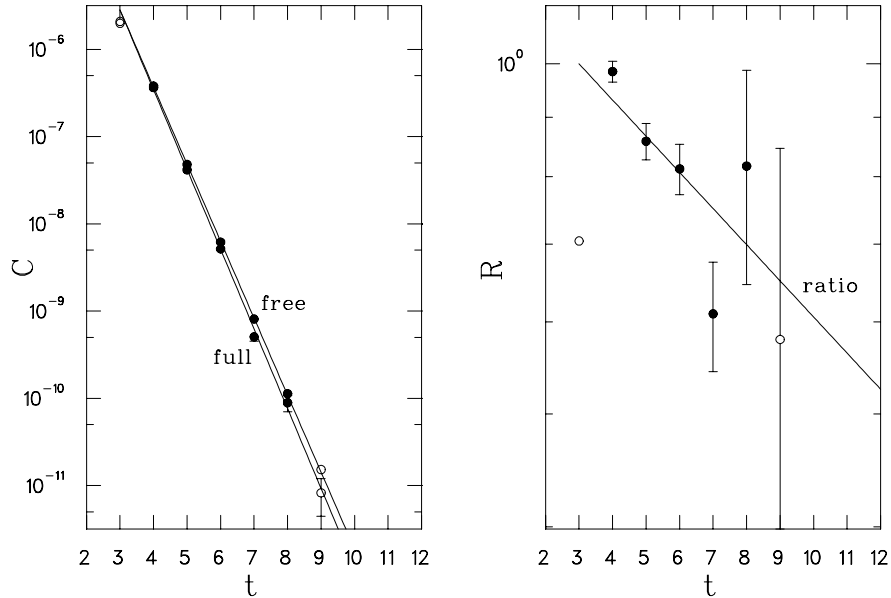


Figure 3: Free and full correlator functions (C) and their ratio (R), for $\beta_1 = 5.720$ and momentum $k = 1$, showing a repulsive mode.

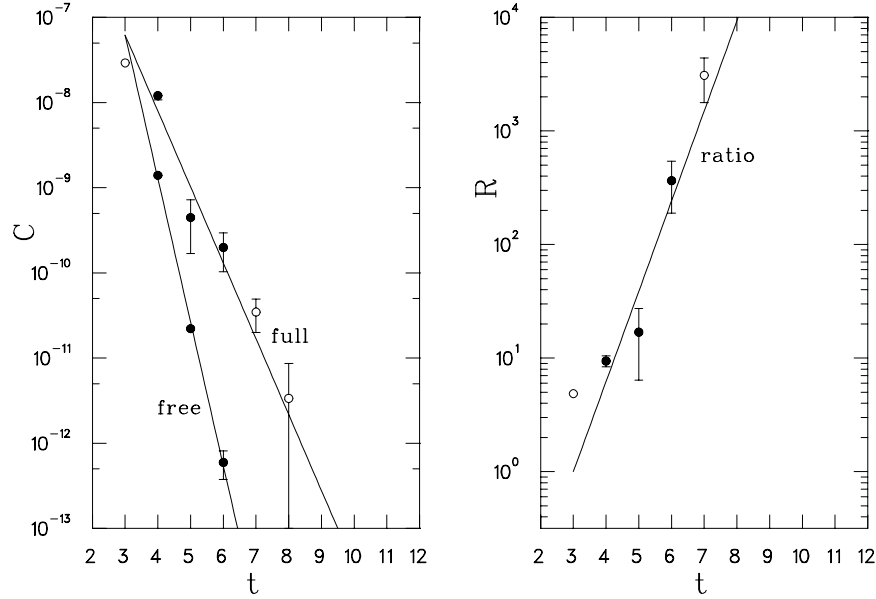


Figure 4: Free and full correlator functions (C) and their ratio (R), for $\beta = 5.720$ and momentum $k = 3$, showing an attractive mode.

diagonal approximation, replacing

$$C_{pq}^{(4;A_1^+)}(t; t_0) \rightarrow \frac{C_{qq}^{(4;A_1^+)}(t; t_0)}{C_{qq}^{(4;A_1^+)}(t_0; t_0)} : \quad (52)$$

Thus the effective correlator becomes

$$C_{qq}^{(4;A_1^+)}(t; t_0) \rightarrow \frac{C_{qq}^{(4;A_1^+)}(t; t_0)}{C_{qq}^{(4;A_1^+)}(t_0; t_0)} ; \quad (53)$$

with off-diagonal elements set to zero.

In Figs. 3 and 4 we show two examples of free and full correlator functions and their ratios, as they appear in (53), both for the smallest inverse hopping parameter, $\beta = 5.720$. The examples are for momenta $k = 1$ and $k = 3$, respectively, see (51). For the repulsive level the mass shift is quite small, which translates into a very noisy signal for the ratio. For the attractive level the mass shift is rather large, however, the falloff of the free correlator function is very steep, which has the effect that only very few time slices are available for analysis. The straight lines in Figs. 3 and 4 come from linear fits to the logarithms of the correlator functions. Only data points marked by filled plot symbols were used in the fits.

The lattice action used here, see Sect. 3.1, exhibits ghosts. These are unphysical branches in the lattice-quark dispersion relation and are indigenous to highly improved actions [38]. The presence of ghosts can contaminate the signal on early time slices.

In our case this contamination is clearly discernible only at $t = 3$. The corresponding data points of the correlator functions have been ignored in our analysis.

Quantum fluctuations manifest themselves in an overall renormalization factor that relates the free and full correlators at $t = t_0$

$$C_{qq}^{(4;A_1^+)}(t_0; t_0) = Z^4 \overline{C}_{qq}^{(4;A_1^+)}(t_0; t_0) : \quad (54)$$

The value obtained from the fits is $Z^4 = 1.97(3)$, or $Z = 1.18$. It is the same for all t , a consequence of the quenched approximation. We have plotted $Z^{-4} C_{qq}^{(4;A_1^+)}(t; t_0)$ in Figs. 3 and 4 to improve readability. Note that Z^4 has no influence on H_I .

3.3 Residual Interaction

In Fig. 5 we show an example of the energy level shifts of the meson-meson system due

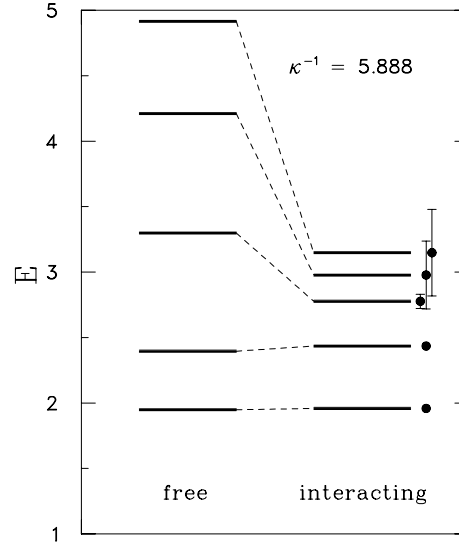


Figure 5: Energy level shifts (hyperfine splittings) due to the residual interaction for the momenta $k = 0; 1; 2; 3; 4$ at a fixed t_0 .

to the residual interaction, for a selected t_0 . Low-momentum (long-distance) modes are weakly repulsive, whereas high-momentum (short-distance) modes are strongly attractive. Errors stem from a bootstrap analysis.

Analyzing the effective correlator (53) along the lines (37)–(39) yields the matrix elements $H_{I;qq}^{(A_1^+)}$. These were used to compute S-wave local potentials $V_0(r)$ according to (46). For the current lattice the sum over on-axis momenta (51),

$$\sum_{\mathbf{q}} \frac{1}{\mathbf{q}^2} \sum_{\mathbf{k} \in \text{ax}} \frac{1}{\mathbf{k}^2} ; \quad (55)$$

truncates at $k_{\text{max}} = 4$. We try to obtain some feel for systematic errors caused by the momentum cut-off k_{max} . On a coarse lattice one should expect those to be large. Thus, in Fig. 6 we show a family of potentials, all for $\kappa^{-1} = 5.888$, which correspond

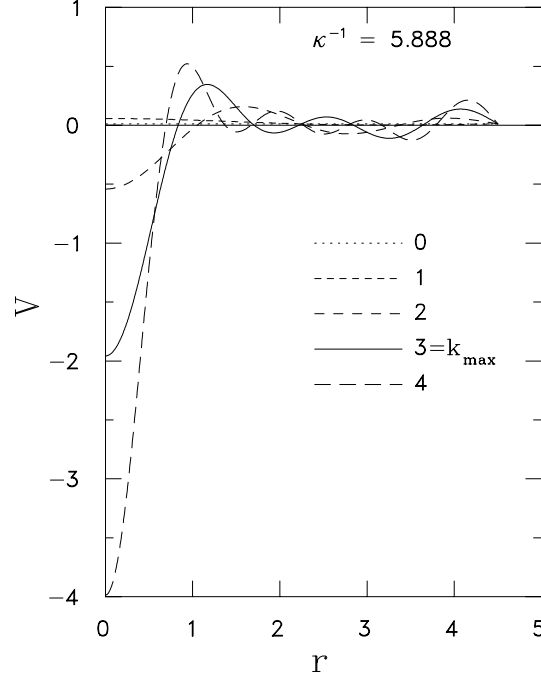


Figure 6: Fourier-Bessel representation (46) of the S-wave local potential, at $\kappa^{-1} = 5.888$. Various momentum truncations, see (55), are shown.

to various upper limits k_{max} .

The matrix elements of the residual interaction (39) depend on the pseudoscalar mass m through the hopping parameter κ . Figure 7 shows $H_{I,qq}^{(A_1^+)}$ as a function of m^2 for momenta $k = 0 :: 4$. The solid lines are three-parameter fits using

$$h_q(x) = h_q + h_q^0 x + h_q^0 x^{3=2} \quad \text{with} \quad x = m^2; \quad (56)$$

which is motivated by chiral perturbation theory [39]. Extrapolation to the chiral limit

$$H_{I,qq}^{(A_1^+)} = h_q(x \rightarrow 0) \quad (57)$$

then yields matrix elements of H_I which describe the residual interaction of the physical $\{ \pi \}$ system in the $I = 2$ channel. We will exclusively refer to those in the subsequent discussion.

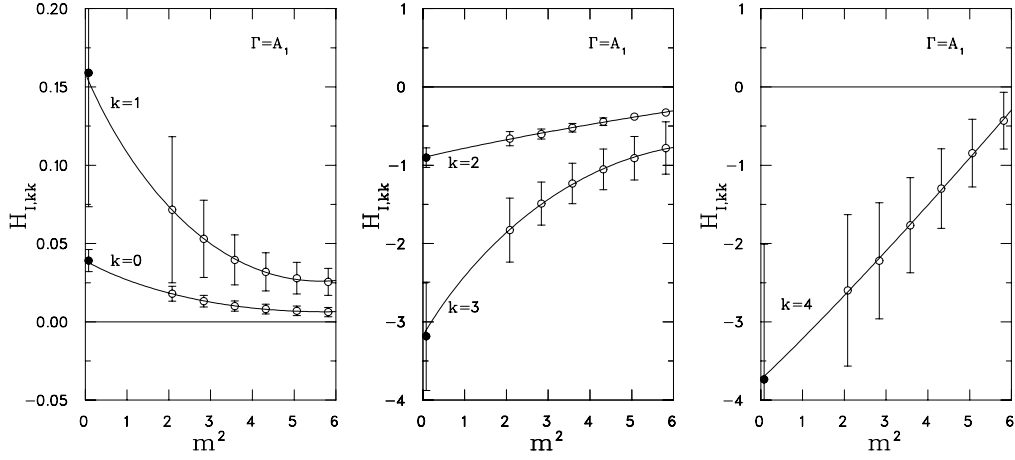


Figure 7: Chiral extrapolations $H_{I,qq}^{(A_1^+)}(m^2 \rightarrow 0)$ for momenta $k = 0 :: 4$, see (51). In physical units the six masses m range from 1.2 to 0.72 GeV, the filled plot symbols refer to $m = 0.14$ GeV.

3.4 Parameterization

In Fig. 8 the solid lines correspond to the extrapolated potentials for $k_{\max} = 3$ and 4, respectively. The oscillations caused by the representation as a truncated Fourier-Bessel series complicate their interpretation.

To get a clearer picture, consider the parametric function

$$V^{(\cdot)}(r) = \frac{1}{1 + \frac{2r^5}{3r^{5+1} \exp(-4r)}} + c_0 \quad \text{where } r \in [0; 1]: \quad (58)$$

It is flexible enough to represent attraction and/or repulsion at certain ranges, and has the feature that the Yukawa form is approached asymptotically,

$$V^{(\cdot)}(r) \rightarrow \frac{1}{3} \frac{e^{-4r}}{r} + c_0 \quad \text{for } r \rightarrow 1: \quad (59)$$

Now define a 'latticeized' version of (58) via

$$V_L^{(\cdot)}(r) = \sum_{k=0}^{k_{\max}} j_0(2q_k r) V_k^{(\cdot)} \quad \text{with } q_k = \frac{2}{L} k: \quad (60)$$

The $V_k^{(\cdot)}$ are expansion coefficients which we have determined from calculating the matrix $B_{lk} = j_0(2q_k r_l)$, with support on $r_0 = 0, r_l = \frac{L}{4(k_{\max} - l + 1)}, l = 1 :: k_{\max}$, and then applying its inverse to (58) as

$$V_k^{(\cdot)} = \sum_{l=0}^{k_{\max}} B_{kl}^{-1} V^{(\cdot)}(r_l): \quad (61)$$

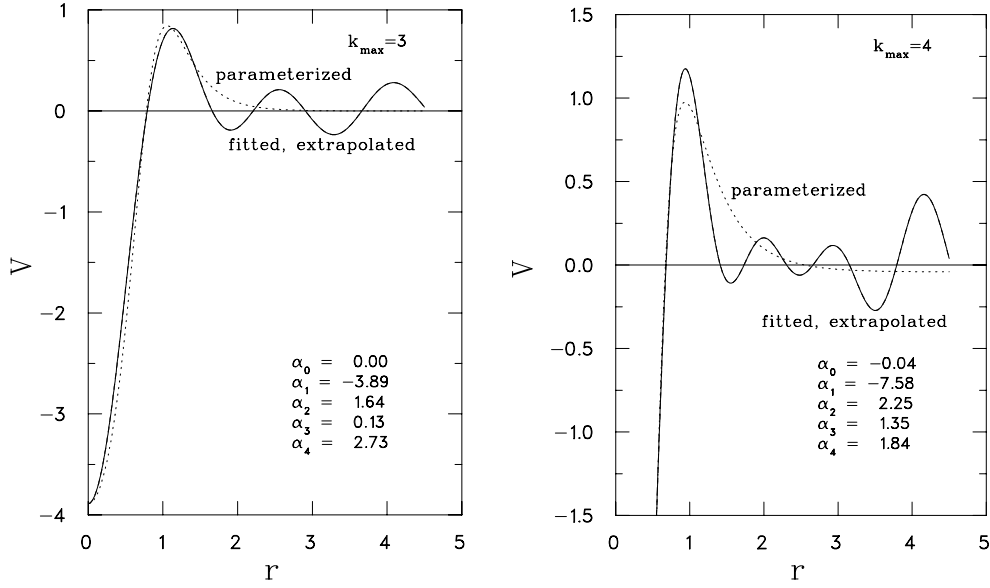


Figure 8: Local potentials for momentum truncations $k_{\text{max}} = 3$ and $k_{\text{max}} = 4$. Shown are the raw lattice results in the $m^2 \rightarrow 0$ limit (extrapolated, solid line), the fits with the Fourier-Bessel trial potential $V_L^{(\cdot)}(r)$ (fitted, solid line), and the corresponding $r \in [0; 1]$ parameterization $V^{(\cdot)}(r)$ (parameterized, dashed line).

In this way the span of $V_L^{(\cdot)}(r)$ is a subspace of the space of functions $V_0(r)$, see (46) and (55), accessible through the lattice simulation. Now make fits to lattice potentials minimizing

$$\int_0^{Z_{L=2}} dr V_0(r) - V_L^{(\cdot)}(r)^2 = \min(\cdot) : \quad (62)$$

We have found that $\gamma_5 = 2$ gives an almost perfect match and thus held this parameter fixed. Also, γ_0 deviates very little from 0 which indicates that the interaction ‘around the world’, across $L a = 3.6 \text{ fm}$, is negligible. The results of the fits are the curves in Fig. 8 marked ‘fitted’. In fact the ‘fitted’ and the ‘extrapolated’ curves are indistinguishable within the line thickness. (This changes if $\gamma_5 \neq 2$.) The curves marked ‘parameterized’ show the corresponding $r \in [0; 1]$ parameterization $V^{(\cdot)}(r)$ as defined in (58).

3.5 Physical Potential

It is tempting to use the resulting fit parameters, shown in Fig. 8, to make contact with the boson-exchange picture of strong interactions, see Fig. 9. This can be done identifying the Yukawa asymptotics (59) of $V(r)$ with

$$m_4 = \frac{1}{4} a^{-1} \cdot 1.4 \{0.9 \text{ GeV} \quad (63)$$

$$\frac{g^2}{4} = \frac{1.2}{3}, 17.4(2.5); \quad (64)$$

see (49). The left and right numbers above relate to $k_{\text{max}} = 3$ and $k_{\text{max}} = 4$, respectively, indicating large systematic errors. Both the mass m_4 of the exchanged particle and the vertex coupling, $g \sim 14.8(5.6)$, are typical for a hadronic system. For example g is around 13.45 for the πN vertex that enters the $N N$ interaction. Statistical errors are also large for these quantities (see Fig. 11).

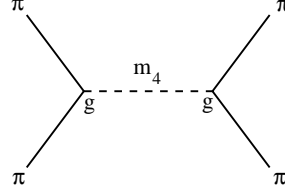


Figure 9: Boson exchange diagram related to (59) and (63), (64).

The above discussion addresses the long-range physics of the system. Figure 10 shows the potentials in the region beyond the lattice cut-off, $r > a$, in physical units. Both truncations at $k_{\text{max}} = 3; 4$ are in agreement and indicate a repulsive residual interaction. In Fig. 11 we show the physical potentials for truncations $k_{\text{max}} = 3; 4$, respectively, together with a family of potentials computed from 8 bootstrap samples. The spread of the dashed lines in Fig. 11 is indicative of the statistical fluctuations. Compared to the $k_{\text{max}} = 3$ case the fluctuations of the $k_{\text{max}} = 4$ potential are visibly larger. A generic feature of two-hadron systems comes to mind as a possible reason. Correlator matrix elements which involve large momenta describe very massive (two-body) states and consequently drop very steeply with time. On small isotropic lattices it is very hard to deal with the resulting deterioration of the lattice signal since data from only very few time slices are usable. From a numerical point of view we consider our results using the truncation $k_{\text{max}} = 3$ the most reliable. Nevertheless, we observe that both momentum cut-off values lead to qualitatively consistent potentials in the long and intermediate range region, $r > 0.4 \text{ fm}$.

The steep drop of the potentials from their values at $r = a$ to deeply negative values at $r = 0$, see Fig. 8, does not influence low-energy physics. It is an indication, however, that the physics in the system at $r = 0$ is special. A possible explanation is suggested by the $SU(3)$ color content of the two-body system. Using standard notation [40, 41] we note that for the color structure of the one-meson interpolating field (1) only the singlet from $\bar{3} \otimes 3 = 8 \oplus 1$ is used. Thus the color-source structure of the two-meson interpolating field (2) is that of an overall singlet, $1 \otimes 1 = 1$. A singlet is also contained in the decomposition of the product of two color octets $8 \otimes 8 = 27 \oplus 10 \oplus 8 \oplus \bar{8} \oplus 10 \oplus 1$.

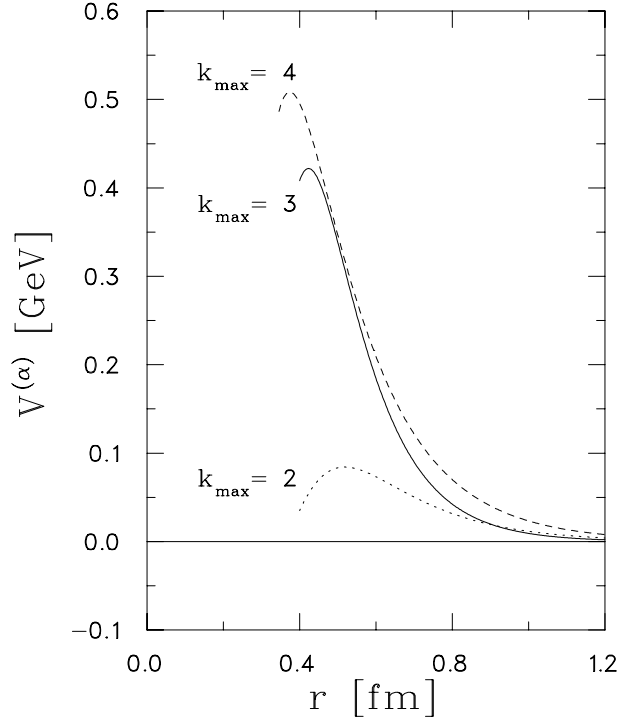


Figure 10: Local potentials for $k_{\text{max}} = 2; 3; 4$ in physical units for distances $r < 0.4 \text{ fm}$.

Naive gluon exchange in 8×8 is attractive [41]. However, in the confinement phase the propagation of the system into an 8×8 color configuration is dynamically suppressed with increasing distance r . This means that we should expect the interaction energy to be more attractive at $r = 0$ as opposed to all other $r = a; 2a; 3a \dots$. The situation is of course more complicated because of dynamical effects from the spin (Dirac) and the flavor degrees of freedom.

In simulations of heavy-light meson-meson systems performed in coordinate space [19] the above mechanism is seen directly. There, the $r = 0$ case can be easily isolated. In our Fourier-Bessel analysis, on the other hand, strong attraction at $r = 0$ can bias the result at $r' = a$ via oscillations of the basis functions. The danger of course is that oscillatory features are misinterpreted as repulsion. We have tried to minimize this by employing the parameterization (58) which would easily be capable of revealing attraction, say at $r = a$, but in fact gives a repulsive interaction in the intermediate and long distance region, $r > a$, as an answer.

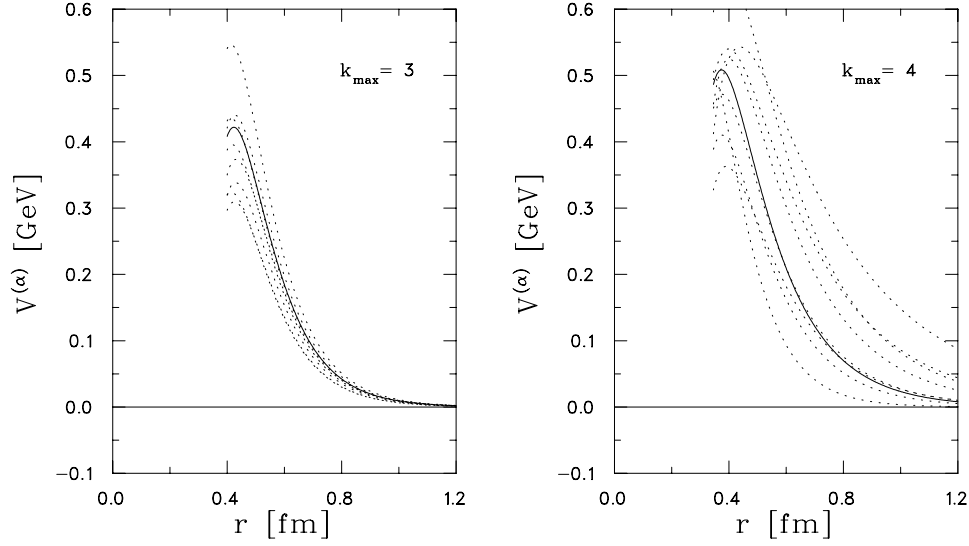


Figure 11: Local potentials for momentum truncations $k_{\text{max}} = 3$ and $k_{\text{max}} = 4$ (solid lines) and families of bootstrap samples (dashed lines) to estimate the overall statistical errors.

3.6 Scattering Phase Shifts

It is obvious that relativistic effects in the $\{\}$ system are very large in the experimentally relevant kinematic region. They are also inherent in the lattice simulation. Nevertheless it is interesting to calculate scattering phase shifts as they arise from the computed potential. This exercise is much in the spirit of section 2.6.1, where it would be based on solving (48) for scattering states. We have used a Volterra integral equation of standard potential scattering theory [42] with $V^{(\alpha)}(r)$ and obtained the scattering phases from Jost functions. The results are shown in Fig. 12, where the two frames distinguish the truncations $k_{\text{max}} = 3; 4$ respectively. The two upper solid curves correspond to the physical reduced mass $m = 2$ of the $\{\}$ system, with $m = 0.28a^{-1} = 0.14 \text{ GeV}$. In order to estimate the magnitude of the error due to the non-relativistic potential scattering theory we have also used the relativistic dispersion relation $m(p) = \sqrt{m^2 + p^2}$. The two lower solid curves in Fig. 12 show the results.

Estimation of the statistical errors on the phase shifts is not a straightforward task and requires some discretion. One option is to select pairs of extremal potentials from the bootstrap analysis of Fig. 11 and compute phase shifts for those. This was done separately for $k_{\text{max}} = 3$ and 4. We have chosen the potentials which stand out in Fig. 11 as the curves with largest and smallest values, respectively, at around $r = 0.6 \text{ fm}$ for $k_{\text{max}} = 3$ and around $r = 0.8 \text{ fm}$ for $k_{\text{max}} = 4$. The resulting phase shifts are shown in Fig. 12 as the boundaries of the dotted regions. Not surprisingly, as discussed above, the

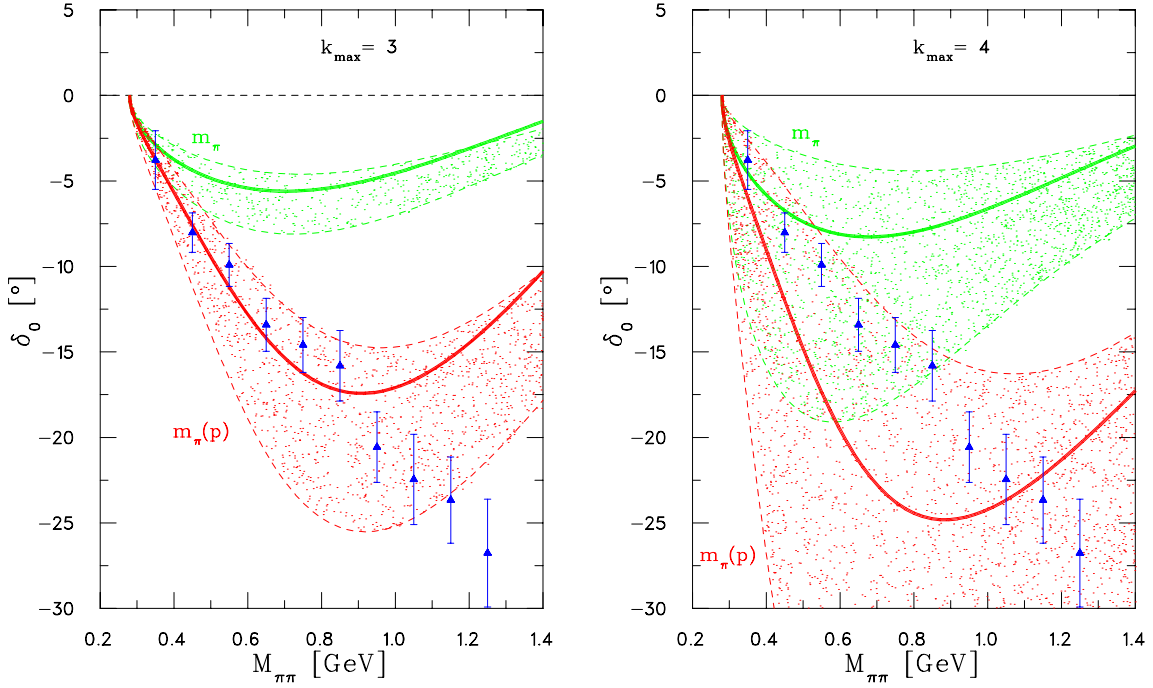


Figure 12: Scattering phase shifts $\delta_0^{I=2}$ calculated from the χ potential of the lattice QCD simulation (thick lines). In uence of m om entum cut-o $k_{\text{max}} = 3$ (left) and $k_{\text{max}} = 4$ (right) is shown. Results using the classical and relativistic dispersion relation are distinguished by m_π and $m_\pi(p)$, respectively. Errors are represented by the dotted regions. Their boundaries (dashed lines) correspond to the phase shifts calculated with extrem al (bootstrap) potentials of Fig. 11. The experim ental data are from [43].

error spread is much larger for $k_{\text{max}} = 4$. Results for both truncations are, nevertheless, consistent.

In the Volterra equation the parameterized potentials $V^{(\chi)}(r)$ were used for the entire interval $r \in [0; 1)$. Their deep attractive trough within $0 < r < a$ is probed by large momenta and is responsible for the scattering phase shifts turning upward beyond $M_\pi > 0.8 - 1.0 \text{ GeV}$. This region is above the lattice cut-off. For smaller M_π the intermediate and long distance region of the potential, essentially as displayed in Fig. 10, is probed. There, it appears that our results are in qualitative agreement with experimental findings. The data points shown as triangles in Fig. 12 are from an analysis of the CERN-Munich $\pi^+\pi^+\pi^0$ experiment by Hoogland et al. [43].

4 Conclusions and Outlook

During the last two decades QCD has emerged as the underlying theory of strong interactions. It is an important problem to put QCD to the test of explaining the interactions between hadrons. The nonperturbative nature of QCD in the energy domain of nuclear physics makes lattice field theory the predestined technique to deal with this question.

We have made an effort in this work to develop and apply lattice QCD techniques to the problem of hadron-hadron interaction. Within the example of a meson-meson system we have outlined a strategy usable to extract a residual interaction from a lattice simulation, which also may point a way to application to other hadronic systems.

On the practical side we have done a simulation of the $\pi^+\pi^+$ system and extracted a local potential for the S-wave interaction. A coarse and large-volume lattice to make space for two hadrons, the extraction of small shifts of energy levels, and steeply declining time correlation functions indigenous to two-hadron states all conspire to make the numerical work rather challenging. Nevertheless, our results indicate a repulsive interaction at long and intermediate ranges, down to $r \approx 0.4\text{fm}$, monotonously rising to $\approx 0.4\text{GeV}$ at that distance. The corresponding scattering phase shifts are subject to large relativistic corrections in the kinematical region of interest, however, within those limitations, they compare favorably with experimental results. The parameterization of our lattice results, matching a Yukawa potential in the asymptotic region, allows us to make contact with traditional boson-exchange models. In this picture we find that the mass of an exchanged particle and its vertex coupling g are in the region of 1GeV and 10, respectively, which are both reasonable for those quantities.

It appears that lattice techniques as tried in the present work are feasible for tackling hadron-hadron interactions. Subsequent work should make use of anisotropic lattices to ease the problems related to steeply dropping correlation functions. It would also be highly desirable to go beyond the 'potential' picture and be able to extract the scattering amplitude (t-matrix) in a more direct fashion numerically from lattice QCD.

Acknowledgement: This work was supported by NSF PHY-9700502, by OTKA T023844 and by FWF P10468-PHY. One of the authors (HRF) is grateful for visiting opportunities at the Institute for Nuclear Physics of the Technical University of Vienna and at Thomas Jefferson Laboratory, where significant advances were made. We thank Nathan Isgur for pointing out [43] to us. The final stages of the work were completed during a most inspiring stay at the Special Research Center for the Structure of Subatomic Matter, CSSM, where the manuscript was written. We would like to thank A.W. Williams for useful discussions on some aspects of scattering related to the lattice.

A Random Sources

We here give details of the random source technique used to compute quark propagator matrix elements and of the smearing procedure.

Consider the linear equation

$$\sum_{\mathbf{y} \mathbf{y}_4} G_{A \mu B}^{-1(f)}(\mathbf{x} \mathbf{x}_4; \mathbf{y} \mathbf{y}_4) X_B^{(f; A^0 \mathbf{r} \mathbf{x}_4^0)}(\mathbf{y} \mathbf{y}_4) = \sum_{A \mu} \sum_{\mathbf{r}} R^{(A^0 \mathbf{r} \mathbf{x}_4^0)}(\mathbf{x}) \delta_{\mathbf{x}_4 \mathbf{x}_4^0}; \quad (65)$$

where $G^{-1(f)}$ is the (known) fermion matrix for flavor f , and R are complex Gaussian random vectors of length L^3 that live on the space sites \mathbf{x} of the lattice. The meaning of the indices are $A; B ::= 1; 2; 3$ color, $\mu ::= 1; 2; 3; 4$ Dirac, $\mathbf{x}; \mathbf{y} ::=$ space ($d = 3$), $\mathbf{x}_4; \mathbf{y}_4$ time, and $\mathbf{r} = 1 :: N_R$ labels the random sources R for each source point. A prime 0 denotes a source point. There is some freedom in choosing the latter. In (65) the sources are nonzero on one time slice $\mathbf{x}_4^0 = t_0$ only. A new source is chosen for each color, Dirac and time index. The same set of sources is used for different flavors (meaning f) in order to take advantage of a multiple-mass solver [35].

A version of a random source technique, called ‘maximal variance reduction’ [44] is currently in use for light-quark propagators in heavy-light systems [20]. There, sources are spread across the entire lattice, including all time slices. Since the variance of the source typically is of order one, exponentially decaying time correlation functions will quickly be engulfed in noise. To alleviate this problem a subdivision of the lattice into disjoint regions, say $0 \leq t < T=2$ and $T=2 \leq t < T$, is made and noise reduction is achieved for propagators connecting those regions, see [44]. On the other hand random sources δ_{t, t_0} , as in (65), avoid the above problem from the outset for lack of noise at the sink. They have proven sufficient in [21] so we continue to employ them here.

The random sources R are normalized according to

$$\sum_{\mathbf{hri}} R^{(A^0 \mathbf{r} \mathbf{x}_4^0)}(\mathbf{x}) R^{(B^0 \mathbf{r} \mathbf{y}_4^0)}(\mathbf{y}) = \delta_{A \mu B \nu} \delta_{\mathbf{x} \mathbf{y}} \delta_{\mathbf{x}_4 \mathbf{y}_4^0}; \quad (66)$$

Here $\langle \dots \rangle_{\mathbf{hri}}^P$ denotes the random-source average, which we approximate numerically as

$$\langle \dots \rangle_{\mathbf{hri}}^P = \frac{1}{N_R} \sum_{r=1}^{N_R} \dots; \quad (67)$$

Employing the solution vectors X of (65) an estimator for the propagator matrix elements then is

$$G_{B \mu A \nu}^{(f)}(\mathbf{y} \mathbf{y}_4; \mathbf{x} \mathbf{x}_4) = \sum_{\mathbf{hri}} X_B^{(f; A \mu \mathbf{r} \mathbf{x}_4)}(\mathbf{y} \mathbf{y}_4) R^{(A \mu \mathbf{r} \mathbf{x}_4)}(\mathbf{x}); \quad (68)$$

Operator smearing [26] is defined through

$$f_{A,0g}^{f0g}(\mathbf{x}t) = f_A(\mathbf{x}) \quad f_{A,0g}^{fsg}(\mathbf{x}t) = \sum_{B, \mathbf{y}} X_{AB}(\mathbf{x};\mathbf{y}) f_B^{fsg}(\mathbf{y}t); \quad (69)$$

with $s \geq N$, and the matrix

$$K_{AB}(\mathbf{x};\mathbf{y}) = A_{B, \mathbf{x}\mathbf{y}} + \sum_{m=1}^{X^3 h} U_{m,AB}(\mathbf{x}t)_{\mathbf{x}\mathbf{y}} + U_{m,AB}^y(\mathbf{y}t)_{\mathbf{x}\mathbf{y}+m} : \quad (70)$$

The real number h and the maximum value S for $s = 0 :: S$ are parameters. We have used fuzzy link variables $U \in SU(3)$ in (70). Due to the linearity of (65) the above iterative prescription translates directly to the random source and solution vectors,

$$R_{C,0}^{f0g(B,0,rt^0)}(\mathbf{z}^0) = \sum_{B, \mathbf{y}} X_{CB}^{f0g} R_{B,0}^{f0g}(\mathbf{y}^0) \quad (\text{no sum over } B^0) \quad (71)$$

$$R_{C,0}^{fsg(B,0,rt^0)}(\mathbf{z}^0) = \sum_{B, \mathbf{y}} X_{CB}^{fsg} K_{CB}^{fsg}(\mathbf{z}^0;\mathbf{y}^0) R_{B,0}^{fsg}(\mathbf{y}^0) \quad (72)$$

$$X_{C,0}^{f0g(f;B,0,rt^0)}(\mathbf{z}t) = \sum_{B, \mathbf{y}} X_{CB}^{f0g} X_{B,0}^{f0g}(\mathbf{y}t) \quad (73)$$

$$X_{C,0}^{fsg(f;B,0,rt^0)}(\mathbf{z}t) = \sum_{B, \mathbf{y}} X_{CB}^{fsg} K_{CB}^{fsg}(\mathbf{z};\mathbf{x}) X_{B,0}^{fsg}(\mathbf{x}t) : \quad (74)$$

Finally, replacing $R \rightarrow R^{fsg}$ and $X \rightarrow X^{fsg}$ in (68) yields the propagator G^{fsg} for smeared fermion fields as used in (5) and (6).

B Elementary Bose Field

Let $\hat{\phi}(\mathbf{x})$ be an elementary Bose field defined on the sites $\mathbf{x} = (\mathbf{x};t)$ of the lattice. It is understood that $\hat{\phi}$ is subject to canonical quantization. Let $\hat{L} = \hat{L}_0 + \hat{L}_I$ be a Lagrangian such that $\hat{L}_0(\hat{\phi};\partial\hat{\phi})$ is the free part and $\hat{L}_I = \hat{L}_I(\hat{\phi})$ is a (small) interaction. Thus \hat{L} gives rise to a Hamiltonian $\hat{H} = \hat{H}_0 + \hat{H}_I$ with according interpretation of its terms. In analogy to (1) and (2) further define $\hat{\phi}_p(t) = L^{-3P} \int d\mathbf{x} e^{ip \cdot \mathbf{x}} \hat{\phi}(\mathbf{x};t)$ and $\hat{\phi}_p(t) = \hat{\phi}_p(t) \hat{\phi}_{+p}(t)$: We have in mind a perturbative calculation of the correlation matrix [21]

$$\hat{C}_{pq}^{(4)}(t;t_0) = h_0 j_p^y(t) \hat{\phi}_q(t_0) j_i \quad (75)$$

assuming a nondegenerate vacuum state j_i with $\hat{H}_0 j_i = 0$. Standard perturbation theory gives rise to the time evolution operator

$$\hat{U}(t;t_0) = \sum_{N=0}^{\infty} \frac{(-1)^N}{N!} \int_{t_0}^t dt_1 \dots \int_{t_0}^t dt_N T[\hat{H}_I(t_1) \dots \hat{H}_I(t_N)]; \quad (76)$$

where $\hat{H}_I(t) = e^{\hat{H}_0(t-t_0)} \hat{H}_I e^{-\hat{H}_0(t-t_0)}$ refers to the interaction picture. Working out (75) with (76) induces a perturbative expansion of the correlator

$$\hat{C}_{pq}^{(4)}(t; t_0) = \sum_{N=0}^{\infty} \hat{C}_{pq}^{(4N)}(t; t_0) : \quad (77)$$

Explicit forms of the $N = 0$ and the $N = 1$ terms are conveniently expressed in terms of wave functions $\psi_n^{(0)}(\mathbf{p})$ defined through

$$c_n^{(0)}(\mathbf{p}) = \langle \mathbf{p} | \hat{H}_I | \psi_n^{(0)} \rangle ; \quad (78)$$

where $\psi_n^{(0)}$ is a complete set of eigenstates of \hat{H}_0 with $\hat{H}_0 \psi_n^{(0)} = W_n^{(0)} \psi_n^{(0)}$, and $c_n^{(0)}$ are appropriate normalization factors chosen such that the $\psi_n^{(0)}$ are orthonormal. The corresponding correlator terms are

$$\begin{aligned} \hat{C}_{pq}^{(4N=0)}(t; t_0) &= \sum_n \psi_n^{(0)}(\mathbf{p}) \psi_n^{(0)}(\mathbf{q}) e^{i(W_n^{(0)}(t-t_0))} \\ \hat{C}_{pq}^{(4N=1)}(t; t_0) &= \sum_n \sum_m \psi_n^{(0)}(\mathbf{p}) \psi_m^{(0)}(\mathbf{q}) \\ &\quad \langle \mathbf{p} | \hat{H}_I | \psi_n^{(0)} \rangle \langle \psi_m^{(0)} | \hat{H}_I | \mathbf{q} \rangle \exp \left[\frac{W_n^{(0)} + W_m^{(0)}}{2} (t - t_0) \right] \\ &\quad + \frac{\sinh \frac{W_n^{(0)} - W_m^{(0)}}{2} (t - t_0)}{\frac{W_n^{(0)} - W_m^{(0)}}{2}} (1 - \delta_{nm}) : \quad (80) \end{aligned}$$

Without loss of generality the normalization constants $c_n^{(0)}$ may be chosen real and positive. We now observe that the two normalization factors and the exponential in (80) may be removed by multiplying $\hat{C}^{(4N=1)}$ from both sides with the inverse square root of $\hat{C}^{(4N=0)}$. Hence the matrix elements of

$$\hat{C}^{(4N=1)}(t; t_0) = \hat{C}^{(4N=0)}(t; t_0)^{-1/2} \hat{C}^{(4N=1)}(t; t_0) \hat{C}^{(4N=0)}(t; t_0)^{-1/2} \quad (81)$$

in the basis $\psi_n^{(0)}(\mathbf{p})$ are products of $\langle \mathbf{p} | \hat{H}_I | \psi_n^{(0)} \rangle$ and the expression inside $\langle : : \rangle$ of (80). The t derivative of the latter is equal to one at $t = t_0$. Thus we have

$$\frac{\partial}{\partial t} \hat{C}_{pq}^{(4N=1)}(t; t_0) \Big|_{t=t_0} = \sum_n \sum_m \psi_n^{(0)}(\mathbf{p}) \langle \mathbf{p} | \hat{H}_I | \psi_n^{(0)} \rangle \psi_m^{(0)}(\mathbf{q}) = \hat{H}_I ; \quad (82)$$

which holds independently of the basis. Finally, we may replace $\hat{C}^{(4N=1)}$ in (81)–(82) with the full correlation matrix $\hat{C}^{(4)}$ since this will only introduce an $N = 2$ error. This leads us to define an effective correlator

$$\hat{C}^{(4)}(t; t_0) = \hat{C}^{(4N=0)}(t; t_0)^{-1/2} \hat{C}^{(4)}(t; t_0) \hat{C}^{(4N=0)}(t; t_0)^{-1/2} : \quad (83)$$

We have shown at this point that $\hat{C}^{(4)}$ has the power series expansion $\hat{C}^{(4)}(t; t_0) = 1 + \hat{H}_I(t - t_0) + O(\hbar^2)$ where the second-order remainder must depend on the product $\hbar = \hat{H}_I(t - t_0)$ for dimensional reasons. In the next order $N = 2$ a calculation similar to the above reveals that

$$\hat{C}^{(4)}(t; t_0) = 1 + \hat{H}_I(t - t_0) + \frac{1}{2} \hat{H}_I(t - t_0)^2 + O(\hbar^3) : \quad (84)$$

Whether or not these are the initial terms of a converging power series expansion for $\hat{C}^{(4)}(t; t_0)$ will depend on the actual H_I . In case the series converges 'everywhere' the expansion will define a correlator even for large $t - t_0$. Limiting ourselves to order $N = 2$ perturbation theory (84) is the same as

$$\hat{C}^{(4)}(t; t_0) = e^{\hat{H}_I(t - t_0)} : \quad (85)$$

The utility of these results in the framework of a lattice simulation lies in the analogy that can be drawn between $\hat{C}^{(4; N=0)}$ and the free correlator $\overline{C}^{(4)}$, and between $\hat{C}^{(4)}$ and the full correlator $C^{(4)}$. The analogue of (85) may then be considered as a definition of an effective interaction.

References

- [1] H. Yukawa, Proc. Phys. Math. Soc. Japan 17 (1935) 48.
- [2] R. Machleidt, Adv. Nucl. Phys. 19 (1989) 189.
- [3] A. Faessler, F. Fernandez, G. Lubeck and K. Shimizu, Nucl. Phys. A 402 (1983) 555.
- [4] D. G. Richards, Nucl. Phys. (Proc. Suppl.) B 9 (1989) 181.
- [5] D. G. Richards, D. K. Sinclair, and D. Sivers, Phys. Rev. D 42 (1990) 3191.
- [6] M. Luscher, Commun. Math. Phys. 105 (1986) 153.
- [7] M. Fukugita, Y. Kuramashi, M. Okawa, H. Mino and A. Ukawa, Phys. Rev. D 52 (1995) 3003.
- [8] M. Luscher, Nucl. Phys. B 354 (1991) 531.
- [9] M. Luscher, Nucl. Phys. B 364 (1991) 237.
- [10] M. Gockeler, H. A. Kastrup, J. Westfalen and F. Zimmermann, Nucl. Phys. B 425 (1994) 413.
- [11] A. M. Green, and P. Pennanen, Phys. Rev. C 57 (1998) 3384.
- [12] P. Pennanen, A. M. Green, and C. Michael, Nucl. Phys. B (Proc. Suppl.) 73 (1999) 351.
- [13] P. Pennanen, A. M. Green, and C. Michael, Phys. Rev. D 59 (1999) 014504.
- [14] A. M. Green, C. Michael, and M. E. Sainio, Z. Phys. C 67 (1995) 291.
- [15] A. M. Green, C. Michael, J. E. Paton and M. E. Sainio, Int. J. Mod. Phys. E 2 (1993) 479.
- [16] A. M. Green, C. Michael and J. E. Paton, Nucl. Phys. A 554 (1993) 701.
- [17] C. Steward and R. Konik, Phys. Rev. D 57 (1998) 5581.
- [18] K. Rabitsch, H. Markum and W. Sakuler, Phys. Lett. 318 B (1993) 507.
- [19] A. Mithal, H. R. Fiebig, H. Markum and K. Rabitsch, Phys. Rev. D 55 (1997) 3077.
- [20] UKQCD Collaboration, C. Michael, and P. Pennanen, Phys. Rev. D 60 (1999) 054012.

- [21] J.D. Canosa and H.R. Fiebig, Phys. Rev. D 55 (1997) 1487.
- [22] H.R. Fiebig, H. Markum, A. Mithaly, and K. Rabitsch, Nucl. Phys. B (Proc. Suppl.) 73 (1999) 252.
- [23] K. Rabitsch, Hadron-Hadron Potentials from Lattice Quantum Chromodynamics, Doctoral dissertation, Technische Universität Wien 1997.
- [24] L. Maiani and M. Testa, Phys. Lett. 245 B (1990) 585.
- [25] M. Cuichini, E. Franco, G. Martinelli and L. Silvestrini, Phys. Lett. 380 B (1996) 353.
- [26] C. Alexandrou, S. Gusken, F. Jegerlehner, K. Schilling and R. Sommer, Nucl. Phys. B 414 (1994) 815.
- [27] S.K. Ma, Statistical Mechanics (World Scientific, Philadelphia - Singapore, 1985).
- [28] M. Luscher and U. Wol, Nucl. Phys. B 339 (1990) 222.
- [29] M. Hamermesh, Group theory and its application to physical problems (Addison-Wesley, Reading, 1964).
- [30] H. Feshbach, Theoretical Nuclear Physics (Wiley, New York, 1992).
- [31] T. Eguchi and N. Kawamoto, Nucl. Phys. B 237 (1984) 609.
- [32] H.W. Hamber and C.M. Wu, Phys. Lett. 133 B (1983) 351.
- [33] H.R. Fiebig and R.M. Woloshyn, Phys. Lett. 385 B (1996) 273.
- [34] F.X. Lee, and D. Leinweber, Phys. Rev. D 59 (1999) 074504.
- [35] U. Glassner, S. Gusken, Th. Lippert, G. Ritzenhoefer, K. Schilling, and A. Frommer, Int. J. Mod. Phys. C 7 (1996) 635.
- [36] H.R. Fiebig, R.M. Woloshyn and A. Dominguez, Nucl. Phys. B 418 (1994) 649.
- [37] C. Albanese et al., Phys. Lett. B 192 (1987) 163.
- [38] M. Alford, T.R. Klassen, G.P. Lepage Nucl. Phys. B 496 (1997) 377.
- [39] J.N. Labrenz and S.R. Sharpe, Nucl. Phys. B (Proc. Suppl.) 34 (1994) 335.
- [40] D.B. Lichtenberg, Unitary symmetry and elementary particles (Academic Press, New York, 1978).

- [41] F.E. Close, An Introduction to Quarks and Partons (Academic Press, New York, 1979).
- [42] J.R. Taylor, Scattering Theory (Wiley & Sons, New York, 1972).
- [43] W. Hoogland, S. Peters, G. Geyer, B. Hyams, P. Weilhammer, W. Blum, H. Dietl, G. Hentschel, W. Koch, E. Lorenz, G. Lütjens, G. Lutz, W. Manner, R. Richter, and U. Stierlin, Nucl. Phys. B 126 (1977) 109.
- [44] UKQCD Collaboration, C. Michael, and J. Peisa, Phys. Rev. D 58 (1998) 034506.

